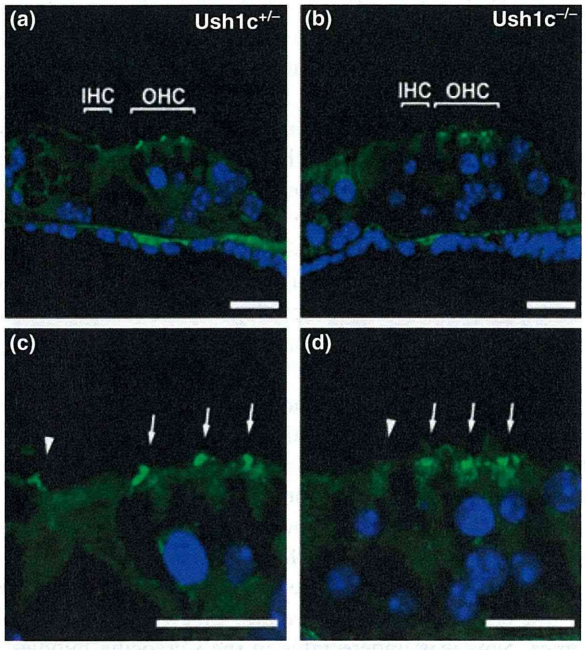

Figure 3 Localization of Sans (green) in the cochlear hair cells of *Ush1c*$^{-/-}$ mice at PD21. Cross sections of the organ of Corti of *Ush1c*$^{+/-}$ (a and c) and *Ush1c*$^{-/-}$ (b and d) mice were stained with an antibody to Sans (green). c and d are higher magnification images of a and b respectively. Arrowheads and arrows indicate inner hair cells and outer hair cells (OHC) respectively. Nuclei were stained by DAPI (Blue). Sans was localized in the stereocilia bundles in *Ush1c*$^{+/-}$ cochlear hair cells at PD21 (c). However, in *Ush1c*$^{-/-}$ mice, strong signals were observed towards the base of stereocilia close to their insertion into the cuticular plate with a slight cytoplasmic staining of OHC (d). Bars indicate 20 μm.

Ush1c$^{-/-}$ mice, characterized by a shift of the immunoreactivity of the proteins towards the base of stereocilia.

Discussion

The USH gene products are part of a protein complex in hair cells of the inner ear. The actin-bundling and PDZ-domain-containing protein harmonin may coordinate the activities of the USH proteins and bridge them to the cytoskeleton of the hair cell (Boeda *et al.* 2002). Disruption of the USH protein network leads to stereociliary disorganization, as observed in mouse models, and is thought to be responsible for congenital deafness in patients with USH (Petit 2001).

Mouse models for USH have played a crucial role in identifying defective genes responsible for USH1 in humans and furthering our understanding of the function of USH1 proteins in normal and disease conditions. All mouse USH1 models are deaf and exhibit vestibular dysfunction. In these mutants, the sensory cells of the cochlea display anomalies in hair bundle development, indicating an essential function for USH1 proteins in stereocilia differentiation (El-Amraoui & Petit 2005). The abnormal stereocilia morphology observed in our *Ush1c* knockout mice is similar to that reported in mouse models for other forms of human USH1.

Regarding spatiotemporal expression, immunohistochemical studies show that the USH1 proteins are expressed in hair cells of the inner ear throughout life. However, USH1 protein subcellular distribution in the stereocilia varies dramatically during development until maturity is reached. Expression of harmonin, Cdh23 and Pcdh15 is detectable in the hair bundle from the moment the bundle emerges at the apical surface of sensory hair cells (Boeda *et al.* 2002; Ahmed *et al.* 2003). Harmonin b is found concentrated at the tips of stereocilia during early postnatal stages but its expression diminishes around PD30 in both the cochlea and vestibule (Boeda *et al.* 2002). The spatiotemporal expression pattern of Cdh23 parallels that of harmonin b, being first observed along the entire length of the emerging stereocilia and then restricted to the tip region.

Notably, Grillet *et al.* (2009) have recently shown that harmonin b is a component of the upper tip-link density, where CDH23 inserts into the stereociliary membrane and is required for normal hair cell mechanoelectrical transduction. In foetal cochlea, Pcdh15 can be detected in supporting cells, outer sulcus cells and the spiral ganglion (Alagramam *et al.* 2001b), while in the mature inner ear, Pcdh15 is also localized in stereocilia of sensory hair cells of both the cochlea and the vestibular organ (Ahmed *et al.* 2003). CDH23 and PCDH15 have been shown to be present in the transient lateral stereocilial and kinocilial links and that the two cadherin proteins interact to form tip-link filaments in sensory hair cells (Sollner *et al.* 2004; Michel *et al.* 2005; Kazmierczak *et al.* 2007). MYO7A is expressed in the mechanosensory hair cells of the vestibular organ and cochlea where it is predominantly localized in the stereocilia, but is also detected within the cuticular plate and the pericuticular necklace region, which is characterized by a dense ring of vesicles (El-Amraoui *et al.* 1996; Hasson *et al.* 1997; Boeda *et al.* 2002).

In this study, we investigated the effect of the *Ush1c* knockout mice on subcellular expression of Myosin 7a, Pcdh15 and Sans in the inner ear. We observed the same distribution of Myosin 7a expression throughout the cytoplasm in knockout and control mice which may indicate that Myosin 7a is expressed earlier than harmonin. This may also suggest that Myosin 7a does not rely on the presence of harmonin isoforms for its cytoplasmic distribution. Whether the cytoplasmic Myosin 7a requires harmonin for hair cells function, however, remains to be examined. We detected Pcdh15 at the base of stereocilia and in the cuticular plate in cochlear hair cells from *Ush1c*$^{+/-}$ controls, whereas in the mutant *Ush1c*$^{-/-}$, Pcdh15 immunoreactivity was found accumulated in the apical region of the OHC and no defined staining was detected at the base of stereocilia nor in the cuticular plate. The scaffold protein Sans has previously been shown localized in the apical hair cell bodies underneath the cuticular plate of cochlear and vestibular hair cells of PD3 mice (Adato *et al.* 2005), but not in the stereocilia. Using an antibody against a peptide sequence corresponding

to the central portion of Sans (amino acid 354–372), we found the protein localized in the stereocilia bundles of mouse cochlear hair cells at PD21 in controls mouse. However, in cochleae from *Ush1c*$^{-/-}$ mice, strong Sans signals were observed towards the base of stereocilia close to their insertion point into the cuticular plate with a slight staining of the cytoplasmic region of OHC. Overall, our data indicated that in mice deficient in harmonin, both interacting partners Pcdh15 and Sans are mislocalized. The epitopes recognized by our antibodies against Pcdh15 and Sans were shifted towards the basal body of the hair cells, whereas they are expressed in the stereocilia of normal control mice.

Acknowledgements

The work is supported by NIH DC05575. We thank Qing Y Zheng for providing *Ush1c* knockout mice DC007392.

References

Adato A., Michel V., Kikkawa Y. *et al.* (2005) Interactions in the network of Usher syndrome type 1 proteins. *Hum. Mol. Genet.* **14**, 347–356.

Ahmed Z.M., Riazuddin S., Bernstein S.L. *et al.* (2001) Mutations of the protocadherin gene pcdh15 cause usher syndrome type 1F. *Am. J. Hum. Genet.* **69**, 25–34.

Ahmed Z.M., Riazuddin S., Riazuddin S., Wilcox E.R. (2003) The molecular genetics of Usher syndrome. *Clin. Genet.* **63**, 431–444.

Alagramam K.N., Yuan H., Kuehn M.H., Murcia C.L., Wayne S., Srisailpathy C.R. (2001a) Mutations in the novel protocadherin pcdh15 cause usher syndrome type 1f. *Hum. Mol. Genet.* **10**, 1709–1718.

Alagramam K.N., Murcia C.L., Kwon H.Y., Pawlowski K.S., Wright C.G., Woychik R.P. (2001b) The mouse ames waltzer hearing-loss mutant is caused by mutation of pcdh15, a novel protocadherin gene. *Nat. Genet.* **27**, 99–102.

Bitner-Glindzicz M., Lindley K.J., Rutland P. *et al.* (2000) A recessive contiguous gene deletion causing infantile hyperinsulinism, enteropathy and deafness identifies the usher type 1c gene. *Nat. Genet.* **26**, 56–60.

Boeda B., El-Amraoui A., Bahloul A. *et al.* (2002) Myosin VIIa, harmonin and cadherin 23, three Usher I gene products that cooperate to shape the sensory hair cell bundle. *EMBO J.* **21**, 6689–6699.

Bolz H., von Brederlow B., Ramírez A. *et al.* (2001) Mutation of CDH23, encoding a new member of the cadherin gene family, causes Usher syndrome type 1D. *Nat. Genet.* **27**, 108–112.

Bork J.M., Peters L.M., Riazuddin S. *et al.* (2001) Usher syndrome 1D and nonsyndromic autosomal recessive deafness DFNB12 are caused by allelic mutations of the novel cadherin-like gene CDH23. *Am. J. Hum. Genet.* **68**, 26–37.

Di Palma F., Holme R.H., Bryda E.C. *et al.* (2001) Mutations in cdh23, encoding a new type of cadherin, cause stereocilia disorganization in waltzer, the mouse model for usher syndrome type 1d. *Nat. Genet.* **27**, 103–107.

El-Amraoui A., Petit C. (2005) Usher I syndrome: unravelling the mechanisms that underlie the cohesion of the growing hair bundle in inner ear sensory cells. *J. Cell Sci.* **118**, 4593–4603.

El-Amraoui A., Sahly I., Picaud S., Sahel J., Abitbol M., Petit C. (1996) Human Usher 1B/mouse shaker-1: the retinal phenotype discrepancy explained by the presence/absence of myosin VIIA in the photoreceptor cells. *Hum. Mol. Genet.* **5**, 1171–1178.

Gibbs D., Kitamoto J., Williams D.S. (2003) Abnormal phagocytosis by retinal pigmented epithelium that lacks myosin VIIa, the Usher syndrome 1B protein. *Proc. Natl Acad. Sci. USA* **100**, 6481–6486.

Gibbs D., Azarian S.M., Lillo C. *et al.* (2004) Role of myosin VIIa and Rab27a in the motility and localization of RPE melanosomes. *J. Cell Sci.* **117**, 6473–6483.

Gibson F., Walsh J., Mburu P. *et al.* (1995) A type VII myosin encoded by the mouse deafness gene shaker-1. *Nature* **374**, 62–64.

Grillet N., Xiong W., Reynolds A. *et al.* (2009) Harmonin mutations cause mechanotransduction defects in cochlear hair cells. *Neuron* **62**, 375–387.

Hasson T., Gillespie P.G., Garcia J.A. *et al.* (1997) Unconventional myosins in inner-ear sensory epithelia. *J. Cell Biol.* **137**, 1287–1307.

Johnson K.R., Gagnon L.H., Webb L.S. *et al.* (2003) Mouse models of ush1c and dfnb18: phenotypic and molecular analyses of two new spontaneous mutations of the ush1c gene. *Hum. Mol. Genet.* **12**, 3075–3086.

Kazmierczak P., Sakaguchi H., Tokita J. *et al.* (2007) Cadherin 23 and protocadherin 15 interact to form tip-link filaments in sensory hair cells. *Nature* **6**, 449.

Kikkawa Y., Shitara H., Wakana S. *et al.* (2003) Mutations in a new scaffold protein sans cause deafness in jackson shaker mice. *Hum. Mol. Genet.* **12**, 453–461.

Lefevre G., Michel V., Weil D. *et al.* (2008) A core cochlear phenotype in ush1 mouse mutants implicates fibrous links of the hair bundle in its cohesion, orientation and differential growth. *Development* **135**, 1427–1437.

Lentz J., Pan F., Ng S.S., Deininger P., Keats B.J. (2007) Ush1c216a knock-in mouse survives katrina. *Mutat. Res.* **616**, 139–144.

Lentz J.J., Gordon W.C., Farris H.E. *et al.* (2010) Deafness and retinal degeneration in a novel USH1C knock-in mouse model. *Dev. Neurobiol.* **70**, 253–267.

Libby R.T., Steel K.P. (2001) Electroretinographic anomalies in mice with mutations in Myo7a, the gene involved in human Usher syndrome type 1B. *Invest. Ophthalmol. Vis. Sci.* **42**, 770–778.

Liu X.Z., Zheng Q.Y., Ouyang X.M., Du L.L., Johnson K.R., Yan D. (2005) Gene targeting and homologous recombination for USH1C gene. *Association for Research in Otolaryngology Meeting*. New Orleans, LA: The Fairmont February, 19–24.

Michel V., Goodyear R.J., Weil D. *et al.* (2005) Cadherin 23 is a component of the transient lateral links in the developing hair bundles of cochlear sensory cells. *Dev. Biol.* **280**, 281–294.

Petit C. (2001) Usher syndrome: from genetics to pathogenesis. *Annu. Rev. Genomics Hum. Genet.* **2**, 271–297.

Smith R.J., Berlin C.I., Hejtmancik J.F. *et al.* (1994) Clinical diagnosis of the Usher syndromes. Usher Syndrome Consortium. *Am. J. Med. Genet.* **50**, 32–38.

Sollner C., Rauch G.J., Siemens J. *et al.* (2004) Mutations in cadherin 23 affect tip links in zebrafish sensory hair cells. *Nature* **428**, 955–959.

Tian C., Liu X.Z., Han F. *et al.* (2010) Ush1c gene expression levels in the ear and eye suggest different roles for Ush1c in neurosensory organs in a new Ush1c knockout mouse. *Brain Res.* **1328**, 57–70.

Verpy E., Leibovici M., Zwaenepoel I. *et al.* (2000) A defect in harmonin, a PDZ domain-containing protein expressed in the inner ear sensory hair cells, underlies usher syndrome type 1C. *Nat. Genet.* **26**, 51–55.

Weil D., Blanchard S., Kaplan J. *et al.* (1995) Defective myosin viia gene responsible for usher syndrome type 1b. *Nature* **374**, 60–61.

Weil D., El-Amraoui A., Masmoudi S. *et al.* (2003) Usher syndrome type 1G (USH1G) is caused by mutations in the gene encoding sans, a protein that associates with the ush1c protein, harmonin. *Hum. Mol. Genet.* **12**, 463–471.

Wilson S.M., Householder D.B., Coppola V. *et al.* (2001) Mutations in cdh23 cause nonsyndromic hearing loss in waltzer mice. *Genomics* **74**, 228–233.

Yan D., Liu X.Z. (2010) Genetics and pathological mechanisms of Usher syndrome. *J. Hum.Genet.* **55**, 327–335.

Yan D., Zheng Q.Y., Ouyang X.M. *et al.* (2006) A gene knockout mouse model for Usher syndrome type 1C. *Association for Research in Otolaryngology Meeting*. Baltimore, February 2006.

Zheng L., Zheng J., Whitlon D.S., García-Añoveros J., Bartles J.R. (2010) Targeting of the hair cell proteins cadherin 23, harmonin, myosin XVa, espin, and prestin in an epithelial cell model. *J. Neurosci.* **30**, 7187–7201.

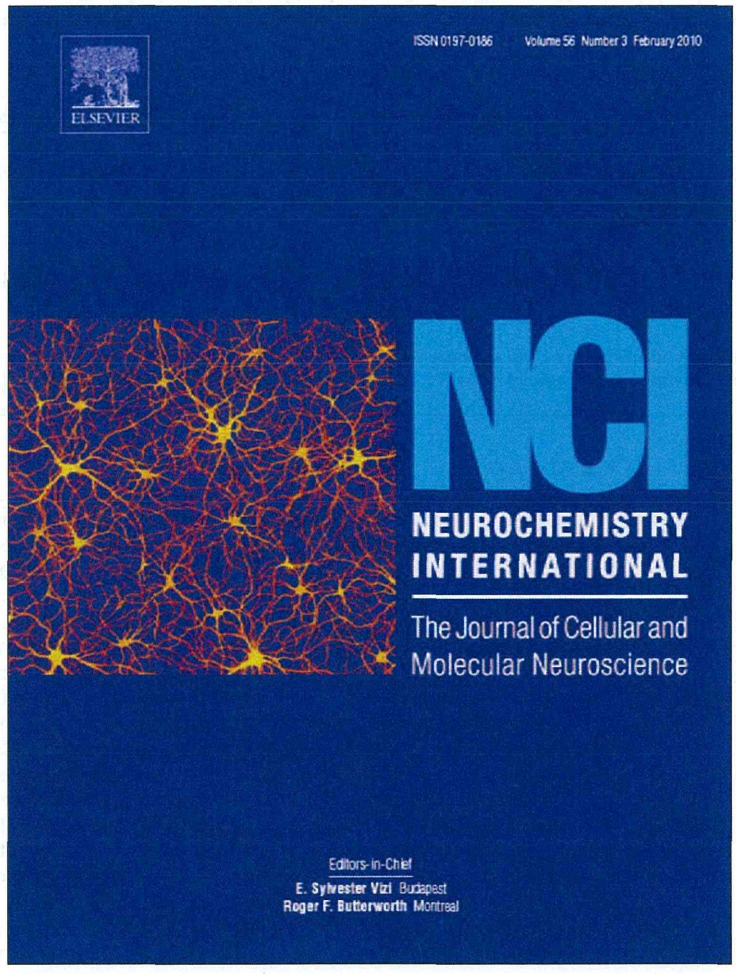

Neurochemistry International 56 (2010) 487–494

Contents lists available at ScienceDirect

Neurochemistry International

journal homepage: www.elsevier.com/locate/neuint

Enhanced expression of C/EBP homologous protein (CHOP) precedes degeneration of fibrocytes in the lateral wall after acute cochlear mitochondrial dysfunction induced by 3-nitropropionic acid

Yoshiaki Fujinami [a], Hideki Mutai [a], Kazusaku Kamiya [a], Kunio Mizutari [a], Masato Fujii [b], Tatsuo Matsunaga [a,*]

[a] Laboratory of Auditory Disorders, National Institute of Sensory Organs, National Tokyo Medical Center, 2-5-1 Higashigaoka, Meguro-ku, Tokyo 152-8902, Japan
[b] Division of Hearing and Balance Research, National Institute of Sensory Organs, National Tokyo Medical Center, Meguro-ku, Tokyo 152-8902, Japan

ARTICLE INFO

Article history:
Received 28 September 2009
Received in revised form 28 November 2009
Accepted 14 December 2009
Available online 21 December 2009

Keywords:
Cochlea
Mitochondria
Apoptosis
Endoplasmic reticulum stress
Oxidative stress

ABSTRACT

We previously reported that treatment of the rat cochlea with a mitochondrial toxin, 3-nitropropionic acid (3-NP), causes temporary to permanent hearing loss depending on the amount of the drug. Furthermore, apoptosis of cochlear lateral wall fibrocytes, which are important for maintaining the endolymph, is a predominant pathological feature in this animal model. 3-NP is known to induce oxidative stress as well as neuronal apoptosis. C/EBP homologous protein gene (*chop*) is one of the marker genes induced during endoplasmic reticulum (ER) stress, and is also considered to be involved in apoptosis. To elucidate the molecular mechanism of cochlear fibrocyte apoptosis induced by 3-NP, we studied spatiotemporal expression of C/EBP homologous protein (CHOP) and other signaling molecules related to ER stress as well as the appearance of apoptotic cells in the cochlear lateral wall after 3-NP treatment. Quantitative real-time PCR revealed that *chop* and activating transcription factor 4 gene (*atf-4*) showed marked increase within 6 h, whereas expression of other ER stress-responsive genes such as *grp78* and *grp94* did not change. Immunohistochemistry showed that 3-NP treatment caused up-regulation of CHOP, especially in type II and type IV fibrocytes, followed by the appearance of terminal deoxynucleotidyl transferase mediated dUTP nick end-labeling (TUNEL)-positive apoptotic cells in the same confined area. Thus, apoptosis of lateral wall fibrocytes induced by 3-NP is likely to be mediated by induction of CHOP. These results contribute clarification of pathological mechanism of cochlear fibrocytes and may lead to development of novel therapeutic strategy for hearing loss.

1. Introduction

Recent advances in auditory research have helped build strategies to cure hearing loss by sensory cell regeneration or prevention of sensory cell loss (Holley, 2005; Kelley, 2006). Most experimental animal models of auditory disorders indicate that noise-induced, hereditary, and drug-induced hearing loss is caused by degeneration of the sensory hair cells or spiral ganglion cells. Recently, several studies reported the involvement of fibrocytes degeneration in the cochlear lateral wall (LW) in hereditary hearing loss (Minowa et al., 1999; Delprat et al., 2005), age-related hearing loss (Spicer and Schulte, 2002), and noise-induced hearing loss (Wang et al., 2002), implying that these non-sensory cells also play important roles in hearing.

We recently established an animal model of acute hearing loss, which is primarily caused by degeneration of LW fibrocytes, using the mitochondrial toxin 3-nitropropionic acid (3-NP) (Hoya et al., 2004; Okamoto et al., 2005; Kamiya et al., 2007; Mizutari et al., 2008). In this model, only less than a 2-fold difference in 3-NP dose differentiates between temporary and irreversible hearing loss. Appearance of TUNEL positive cells (Kamiya et al., 2007; Mizutari et al., 2008), and blockade of fibrocyte degeneration by caspase inhibitor (Mizutari et al., 2008) indicate that degeneration of LW fibrocytes is mainly apoptosis in this model. LW fibrocytes are critical for maintaining the ion concentration of the endolymph by K^+ recycling from the perilymph (Schulte and Steel, 1994; Spicer and Schulte, 1998); and disturbance of the endolymphatic ion concentration leads to immediate hearing loss. Fibrocytes of the LW are divided into five cell types based on structural features, immunostaining patterns and general location (Schulte and Adams, 1989; Spicer and Schulte, 1996; Mutai et al., 2009). Type II and type IV fibrocytes contain numerous mitochondria, and endoplasmic

* Corresponding author. Tel.: +81 3 3411 0111; fax: +81 3 3411 0185.
E-mail address: matsunagatatsuo@kankakuki.go.jp (T. Matsunaga).

0197-0186/$ – see front matter © 2009 Elsevier Ltd. All rights reserved.
doi:10.1016/j.neuint.2009.12.008

reticulum (ER) expresses various types of ion transporters, channels, and pumps, and have significant roles in maintenance of the endolymph. 3-NP is considered to elicit acute deafness by depleting energy in the cochlea, which primarily induces apoptosis of type II and type IV fibrocytes followed by perturbation of endolymph homeostasis. Understanding the molecular pathway of LW fibrocytes cell death is likely to provide insight for preventing auditory disorders caused by LW fibrocyte dysfunction.

3-NP administration alters gene expression in various tissues and induces apoptosis in neuronal cells (Behrens et al., 1995; Pang and Geddes, 1997; Sato et al., 1997). C/EBP homologous protein (CHOP) is a DNA binding protein targeted by activating transcription factor 4 (ATF-4). *chop* (encoding CHOP) is one of the marker genes induced in ER stress (Oyadomari and Mori, 2004), which was originally defined as a cellular response against accumulation of unfolded proteins in the ER (Xu et al., 2005). In addition, the accumulation of unfolded proteins in mitochondria also induces CHOP expression (Zhao et al., 2002). CHOP is considered to be involved in apoptosis in various cell types (Matsumoto et al., 1996; Maytin et al., 2001). Part of the downstream pathways of CHOP that leads to apoptosis was recently revealed. It was reported that overexpression of Bcl-2 blocks CHOP-induced apoptosis (Matsumoto et al., 1996), Tribbles-related protein 3 (TRB3) repress the transcriptional activity of CHOP (Ohoka et al., 2005) and Bcl-2 interacting mediator of cell death (Bim) is closely related to the CHOP-induced apoptosis (Puthalakath et al., 2007). CHOP expression is induced in Parkinson's disease (Holtz and O'Malley, 2003), ischemia–reperfusion injury (Tajiri et al., 2004), and diabetes (Araki et al., 2003). The linkage between CHOP induction and cell death raises the possibility that CHOP may also play a role in eliciting apoptosis of LW fibrocytes exposed to 3-NP. To explore this possibility, we examined the induction of CHOP and other ER stress-related molecules such as *atf-4* gene (encoding an ATF-4) in the LW of 3-NP-treated animals, and the relationship of CHOP expression and apoptosis in the degenerating cells.

2. Results

2.1. Time course of hearing after 3-NP treatment

The time course of hearing in rats treated with 3-NP was measured by auditory brainstem response (ABR). Because our previous studies using the same animal model as the present study showed a remarkable difference in the time course of ABR thresholds at 8 kHz and 20 kHz between TTS and PTS rats, we measured ABR thresholds at these two frequencies in the present study. The rats treated with 300 mM 3-NP demonstrated severe hearing loss at both 8 kHz and 20 kHz (72.0 ± 5.9 dB and 85.5 ± 1.5 dB, respectively) 1 day after the treatment (DAT, Fig. 1). At 7 DAT, the threshold shift at 8 kHz recovered to almost the normal range (15.0 ± 1.2 dB) and the threshold shift at 20 kHz gradually recovered to a moderate level of hearing loss (40.0 ± 8.9 dB). These rats were referred as temporary threshold shift (TTS) rats. In contrast, the ABR threshold in rats treated with 500 mM 3-NP exceeded the highest measurable level at both tested frequencies 3 h after the treatment and did not show any signs of recovery even at 7 DAT. These rats were referred as permanent threshold shift (PTS) rats. Saline-treated rats maintained normal thresholds, indicating that the surgical procedures did not cause hearing loss. These phenotypes were consistent with our previous data (Hoya et al., 2004).

2.2. Time course of chop and atf-4 expression in the LW after 3-NP treatment

To explore the molecular events during hearing loss by 3-NP, we investigated whether the genes activated during ER stress were

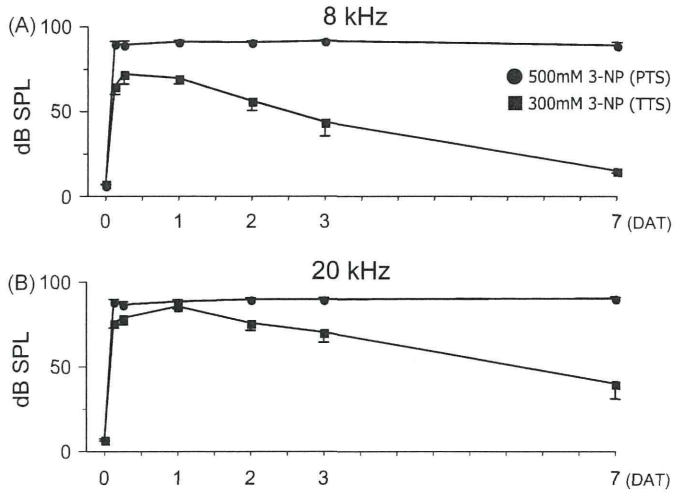

Fig. 1. Time course of auditory thresholds in temporary threshold shift (TTS) rats treated with 300 mM 3-nitropropionic acid (3-NP) and permanent threshold shift (PTS) rats treated with 500 mM 3-NP. The threshold shifts were recorded at 8 kHz (A) and 20 kHz (B). Although the thresholds reached their peak at 1 day after 3-NP treatment (DAT) and then decreased in the TTS rats, the thresholds in the PTS rats exceeded the measurable levels at 3 h after the treatment and were stable at 7 DAT. $n = 5$.

up-regulated in the LW after 3-NP treatment. Expression of four ER stress-responsive genes (*chop*, *atf-4*, *grp78*, and *grp94*) along with the housekeeping gene glyceraldehyde-3-phosphate dehydrogenase (*gapdh*) in the cochlear middle turn of TTS and PTS rats was measured using semi-quantitative reverse transcription PCR (RT-PCR). LW of cochlear middle turn was chosen because histological changes indicating degeneration of LW fibrocytes were evidently detected at this region in both TTS and PTS rats and there was a remarkable difference in the time course of ABR thresholds at this region between TTS and PTS rats.

We found that all five transcripts were successfully amplified in the LW from untreated rats (Fig. 2A). In addition, two of them, *chop* and its activator *atf-4*, both of which are suggested to be involved in activation of the apoptotic pathway, were up-regulated after 3-NP treatment. The changes in *chop* and *atf-4* expression from 3 h to 7 DAT were similar in the TTS and PTS rats; an increase of the PCR bands occurred in TTS and PTS rats within a few hours after treatment, but these band intensities dropped to the untreated levels in TTS rats and even lower in PTS rats at 1 DAT. In contrast, expression of *grp78* and *grp94*, molecular chaperones in the ER lumen and indicators of cell survival (Kaufman, 1999), did not show apparent changes throughout the experimental period (Fig. 2A), indicating that not all the genes mediating ER stress are stimulated in the LW after 3-NP treatment.

In the next experiment, expression levels of *chop* and *atf-4* after 3-NP treatment from which the changes were seen in the RT-PCR results were further evaluated by quantitative real-time RT-PCR (qPCR). These gene expressions were compared with those in untreated rats (0 DAT, $n = 5$). Because neither *grp78* nor *grp94* expression did not change in the screening by RT-PCR, these gene expressions were not measured by qPCR. The level of *chop* (Fig. 2B) was increased at 6 h after the treatment (390 ± 91% in TTS rats, $p < 0.05$, and 595 ± 262% in PTS rats), confirming our previous observation that *chop* is induced promptly after 3-NP treatment. However, no significant difference in the peak level of *chop* was observed between PTS and TTS rats. At 1 DAT, the *chop* level dropped sharply to 53 ± 6% in TTS rats and 58 ± 16% in PTS rats, followed by gradual recovery to the untreated level in TTS and PTS rats until 7 DAT. As observed for *chop*, *atf-4* expression significantly increased and reached its peak 6 h after 3-NP treatment (Fig. 2C). The increase in *atf-4* expression was lower than that in *chop* both in TTS rats

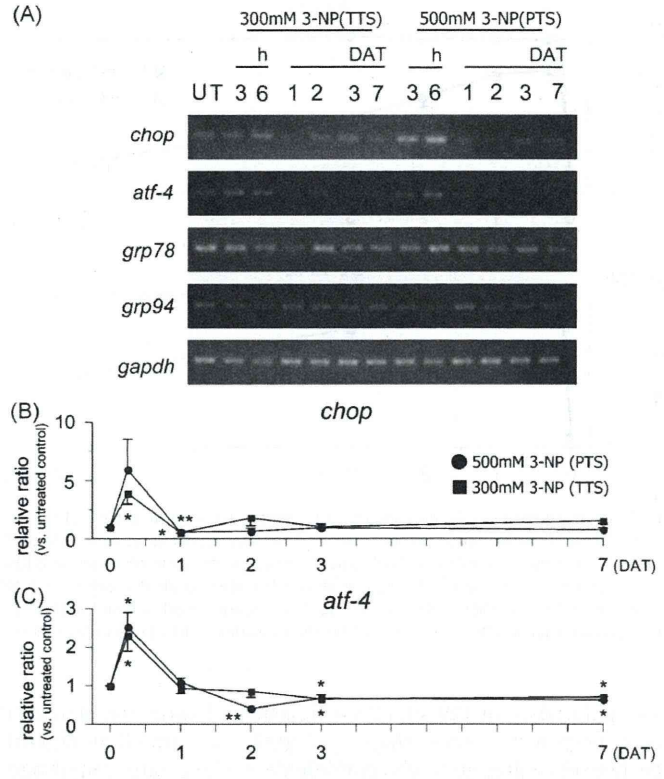

Fig. 2. Expression of ER stress-responsive genes in the lateral wall (LW) after 3-NP treatment. Expression was determined by semi-quantitative reverse transcription PCR (A) and quantitative real-time PCR (B and C). UT; untreated control rats; *gapdh*; glyceraldehyde-3-phosphate dehydrogenase. DAT; day(s) after 3-NP treatment. *chop* (B) and *atf-4* (C) were temporarily induced in the LW 6 h after treatment in both TTS rats treated with 300 mM 3-NP and PTS rats treated with 500 mM 3-NP. *chop* was decreased to approximately half of the untreated level (0 h) at 1 DAT and then recovered to the normal level. $n = 5$. $^{*}p < 0.05$, $^{**}p < 0.01$, significant difference vs. untreated control.

($230 \pm 40\%$, $p < 0.05$) and in PTS rats ($252 \pm 38\%$, $p < 0.05$). In the TTS and PTS rats, *atf-4* was down-regulated to $71 \pm 10\%$ and $64 \pm 8\%$ of the untreated level, respectively, at 7 DAT. Taken together, *chop* and *atf-4*, which are activated by various stimuli including ER stress, were responsive to 3-NP in the present study, whereas expression of the other candidate genes, *grp78* and *grp94*, did not change in response to the treatment.

2.3. Spatial expression patterns of CHOP and apoptosis in the LW after 3-NP treatment

We next investigated spatial expression patterns of the CHOP in the LW after 3-NP treatment. CHOP signals were detected using immunohistochemistry with paraformaldehyde-fixed, paraffin-embedded tissues. We focused on the cochlear middle turn to compare with expression levels of *chop* and *atf-4* by RT-PCR and qPCR. The same primary antibody for CHOP was used in this study as that used for a previous report (Hayashi et al., 2005). To ascertain specific binding of the primary antibody, a set of sections was stained in a similar way without the primary antibody, and the staining was not detected (data not shown). Types of LW fibrocytes were judged based on their localization within the spiral ligament according to the previous studies (Schulte and Adams, 1989; Spicer and Schulte, 1996; Mutai et al., 2009). Fig. 3 shows distribution of the CHOP signal at the middle turn of the LW before and after 3-NP treatment. CHOP was detected at low levels in the LW of untreated and saline-treated rats (Fig. 3A and F). The low CHOP signal level persisted until 6 h after treatment in both TTS and PTS rats (Fig. 3B and G). The CHOP signal intensity started to increase over the entire spiral ligament at 1 DAT in both TTS and PTS rats (Fig. 3C and H), with the most intense staining in the area of type II and type IV fibrocytes in PTS rats. At this time in the TTS, CHOP immunoreactivity was localized mainly in the cytoplasm (Fig. 3C and L), and localized slightly also in the nuclei. CHOP immunoreactivity did not remain in the LW at 2 DAT (Fig. 3D). On the other hand, immunoreactivity in the PTS rats at 1 DAT was localized mainly in the nuclei (Fig. 3H and N), and remained in the LW at 2DAT and 3 DAT (Fig. 3I and J). Fibrocyte degeneration was not apparent in the spiral ligament of either TTS or PTS rats until 1 DAT. In TTS rats, fibrocyte degeneration which was indicated by a region free of cellular nuclei was observed in the area of type II and type IV fibrocytes at 2 DAT (Fig. 3D and M) and 3 DAT (Fig. 3E) and area of fibrocyte degeneration did not expand from 2 DAT to 3 DAT. In PTS rats, a subpopulation of type II and type IV fibrocytes started to disappear and CHOP immunoreactivity was detected around this area at 2 DAT (Fig. 3I and O), and a majority of the fibrocytes in the LW had degenerated at 3 DAT (Fig. 3J).

Because our previous study showed that death of LW fibrocytes is mediated by an apoptotic pathway (Kamiya et al., 2007; Mizutari et al., 2008), we next investigated whether the onset of apoptotic cell death coincides with the onset of CHOP induction. The paraffin sections were used for the terminal deoxynucleotidyl transferase mediated dUTP nick end-labeling (TUNEL) assay, a method generally accepted to detect DNA fragmentation caused by activation of apoptotic pathways (Fig. 4). TUNEL-positive cells were not detected in untreated and saline-treated LWs (Fig. 4A and F). In TTS rats (Fig. 4B–E), TUNEL-positive cells appeared at 2 DAT in the area of type II fibrocytes (Fig. 4D and M). A small number of TUNEL-positive cells were also evident at 3 DAT (Fig. 4E). In PTS rats (Fig. 4G–J), TUNEL-positive cells were detectable as early as 1 DAT in the type II/IV fibrocytes (Fig. 4H). The number of TUNEL-positive cells in the LW gradually increased from 1 to 3 DAT (Fig. 4H–J). To clarify whether CHOP induction and apoptotic cell death are associated, the LWs in the untreated or PTS rats were subjected to a double immunofluorescence study (Fig. 5A–J). CHOP signal (red) was low in untreated rats (Fig. 5A, D, E) and intensified in the area of type II and type IV fibrocytes at 1 DAT in PTS rats (Fig. 5F, I, and J). TUNEL-positive apoptotic cells (green) were undetectable in the LW of untreated rats (Fig. 5B, D, and E) but were observed in PTS rats at 1 DAT (Fig. 5G, I, and J). Although apoptotic cells were not convincingly co-immunostained with CHOP in PTS rats at 1 DAT, they were confined to the CHOP-positive area (Fig. 5I and J). In untreated rats, the CHOP signal visualized by fluorescein staining in the stria vascularis (Fig. 5A) was inconsistent with the absence of a signal in the stria vascularis by 3,3′-diaminobenzidine (DAB) staining (Fig. 3A). The difference was considered to be due to the methods used for antigen retrieval. Because apoptotic cells were not detected in the stria vascularis, we focused on the CHOP expression in the spiral ligament. Thus, CHOP expression in the stria vascularis is not discussed further in this study. Overall, we demonstrated that induction of the CHOP signal was followed by apoptotic cell death in the LW fibrocytes after 3-NP treatment.

3. Discussion

In this study, we examined the time course of CHOP expression, apoptosis, and degeneration of fibrocytes after administration of 3-NP. We demonstrated temporary CHOP expression in the confined area of LW in which fibrocyte degeneration occurred afterwards. In TTS rats, TUNEL-positive cells became detectable at 2 DAT, approximately 1 day after CHOP induction. In PTS rats, a few TUNEL-positive cells were detectable at 1 DAT, when the CHOP level was first up-regulated. Then, the number of TUNEL-positive cells increased significantly at 2 DAT. CHOP and TUNEL signals are detectable in the same area, but co-localization of these two

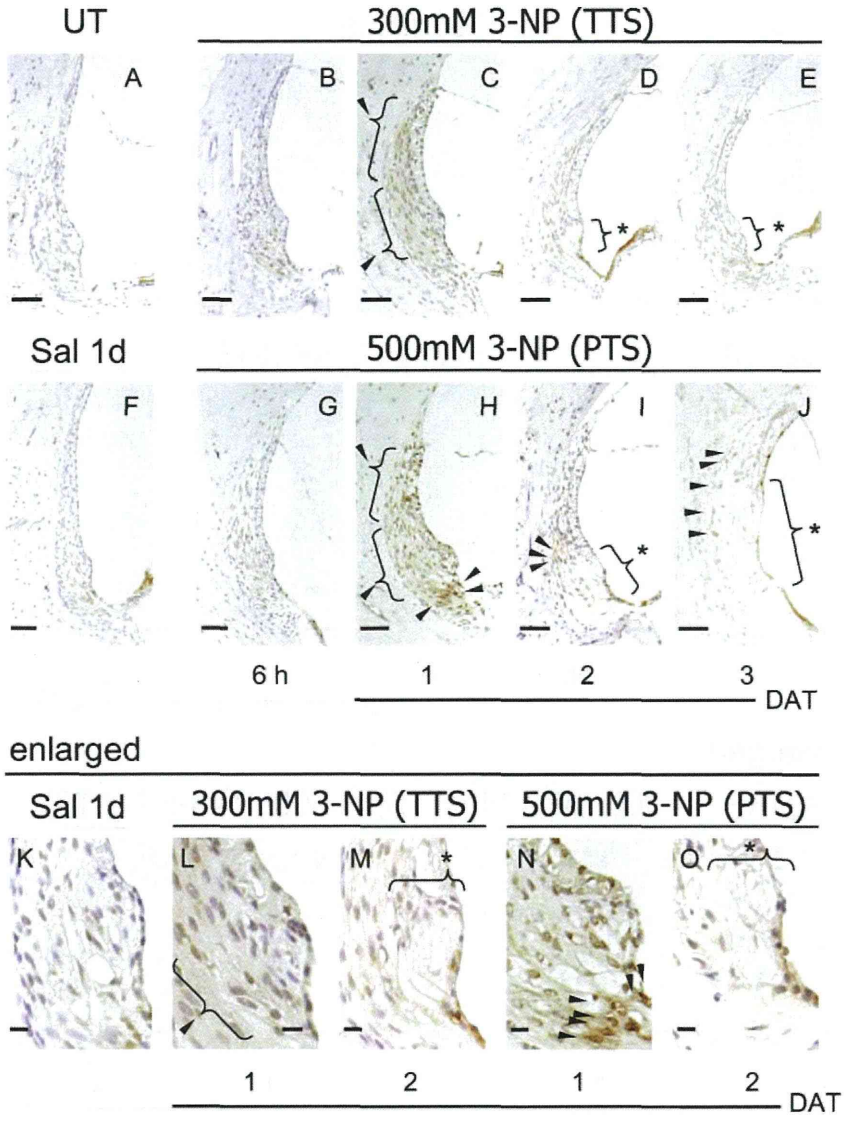

Fig. 3. Immunohistochemical analysis of CHOP expression in the LW after 3-NP treatment. In untreated control rats (UT), a low level of CHOP was detectable in the entire LW (A). In TTS rats treated with 300 mM 3-NP (B–E, L, and M), the CHOP signal (arrowheads) was unchanged at 6 h but intensified 1 day after 3-NP treatment (DAT) (C) compared with saline-treated rats (Sal 1d, F, K). A limited area (asterisk) of the LW had degenerated at 2 DAT and 3 DAT (D, E). In PTS rats treated with 500 mM 3-NP (G–J, N, and O), an intense CHOP signal (arrowheads) was evident, especially in the area of type II and type IV fibrocytes of the LW at 1 DAT (H). At 2 DAT, type II and type IV fibrocytes appeared to start degeneration (asterisk) (I), and the area of degenerated fibrocytes expanded at 3 DAT (J). K–O are enlarged images of spiral prominence of F, C, D, H and I, respectively. Scale bar = 50 μm (A–J) and 10 μm (K–O).

staining was not detected. Because CHOP is known to be involved in inducing apoptosis (Matsumoto et al., 1996; Maytin et al., 2001), we speculate that the delay of TUNEL appearance is due to signal transduction for apoptotic pathways. Tajiri et al. (2004) reported that *chop* induction in the striatum peaks 12 h after the occlusion of the carotid artery, followed by detection of numerous TUNEL-positive cells at 24 h. Investigation of signaling molecules downstream of CHOP (Wang et al., 1998; Sok et al., 1999) and activation of pro-apoptotic molecules such as caspases after 3-NP treatment may clarify the direct association of CHOP activation with apoptotic cell death in LW fibrocytes. In the present study, of note is that nuclei were also positively stained for CHOP in PTS rats at 1 DAT, which is required to exert functional effect for this transcription factor (Zinszner et al., 1998).

The activation of ATF-4 and CHOP in the LW of 3-NP-treated rats is reminiscent of CHOP and ATF-4 activation in ischemic brain (Hayashi et al., 2005). Induction of the same molecules in these two affected areas is probably caused by the features of energy depletion which are shared by mitochondrial dysfunction and ischemia. What is the mechanism of the expression of *atf-4* and CHOP which is the downstream target of ATF-4 in LW fibrocytes? The mitochondrial toxin 3-NP is an irreversible inhibitor of succinate dehydrogenase (complex II of the electron transport chain) (Coles et al., 1979). Inhibition of energy metabolism by 3-NP results in the production of reactive oxygen species (Beal et al., 1995; Lee et al., 2002; Rosenstock et al., 2004) that causes oxidative stress and neuronal cell death (Behrens et al., 1995; Pang and Geddes, 1997; Sato et al., 1997; Higuchi, 2004). Oxidative stress induces ER stress (Yu et al., 1999), and this is known to enhance CHOP expression (Oyadomari and Mori, 2004). In addition, cells exposed to 3-NP also release mitochondrial Ca^{2+}, which is caused by an increasing amount of reactive oxygen species (Rosenstock et al., 2004) and rapid elevation of the intracellular Ca^{2+} level is known to enhance CHOP expression (Deshpande et al., 1997; Tanaka et al., 2005). Thus, oxidative stress, ER stress and increase in the intracellular Ca^{2+} level are related events in terms of the molecular signaling pathways. We assume 3-NP induced ATF-4 and CHOP in LW by these mechanism.

Our findings are not in full agreement with the hypothesis that CHOP is activated exclusively in response to ER stress in the LW

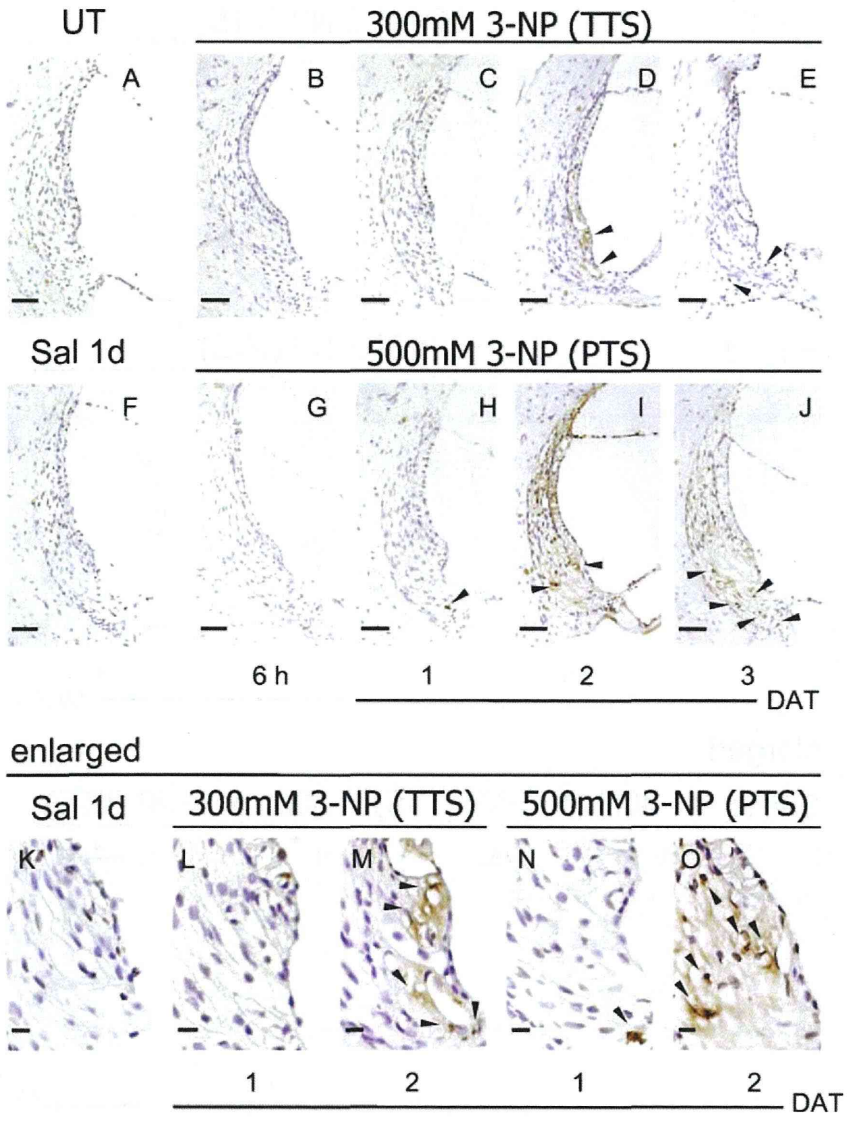

Fig. 4. TUNEL histochemical analysis of apoptotic cells in the LW after 3-NP treatment. Apoptotic cells were not detected in untreated control rats (UT; A) or in saline-treated rats (Sal 1d; F). In TTS rats treated with 300 mM 3-NP (B–E), a small number of apoptotic cells (arrowheads) were found at 2 DAT and 3 DAT (D, E). In PTS rats treated with 500 mM 3-NP (G–J), apoptotic cells were detectable at 1 DAT (H). The number of apoptotic cells (arrowheads) increased as the degenerating area expanded at 2 DAT and 3 DAT (I, J). K–O are enlarged images of spiral prominence of F, C, D, H and I, respectively. Scale bar = 50 μm (A–J) and 10 μm (K–O).

treated with 3-NP, because multiple attempts failed to show significant up-regulation of the ER stress mediators *grp78* and *grp94*. These results suggest that either a partial ER stress-response pathway including ATF-4 and CHOP is activated, or that mechanisms other than ER stress are responsible for the activation of the two molecules in the LW treated with 3-NP. CHOP has been reported to be induced without activation of other ER stress-responsive proteins such as GRP78 in a cultural experimental model of mitochondrial stress (Zhao et al., 2002). In this model, accumulation of unfolded proteins in the mitochondria resulted in induction of CHOP and mitochondrial molecular chaperones (e.g., Cpn60, Cpn10 and mtDnaJ), but did not induce non-mitochondrial chaperones including GRP78. Moisoi et al. (2009) also reported that *chop* expression was increased by mitochondrial dysfunction in the brain. Similarly, induction of *atf-4* and *chop* in the LW after 3-NP treatment may also be caused by mitochondrial stress following oxidative stress. On the other hand, investigation of PERK, IRE-1 and ATF-6 is necessary to demonstrate that ER stress is concerned with the increase of *chop* expression in this study.

The expression levels of *chop* at 6 h after 3-NP treatment and at 1 DAT were not significantly different between TTS and PTS rats, despite the contrasting number of degenerating cells at 3 DAT. Immunohistochemical study revealed nuclear staining of CHOP, which is required to undergo functional role for transcription factor, in PTS rats but rarely in TTS rats. This may explain the different levels of apoptosis at 3 DAT. Another possibility is that CHOP may be involved in the only initial induction of apoptosis in this model and another death pathway which sustained ongoing cell death was also activated in PTS rats but not activated in TTS rats. Further study to identify regulators of degeneration in LW fibrocytes will provide us with insight to develop strategies to prevent death of LW fibrocytes.

In summary, we characterized a novel molecular mechanism of acute hearing loss caused by 3-NP administration and identified CHOP, a mediator of oxidative stress, ER stress, and mitochondrial stress, as a preceding marker of damage in LW fibrocytes.

4. Experimental procedures

4.1. Animals and drug administration

Male Sprague–Dawley rats (6–8 weeks old, weighing 170–230 g) were used. The rats were housed in metallic breeding cages in a room with a light/dark

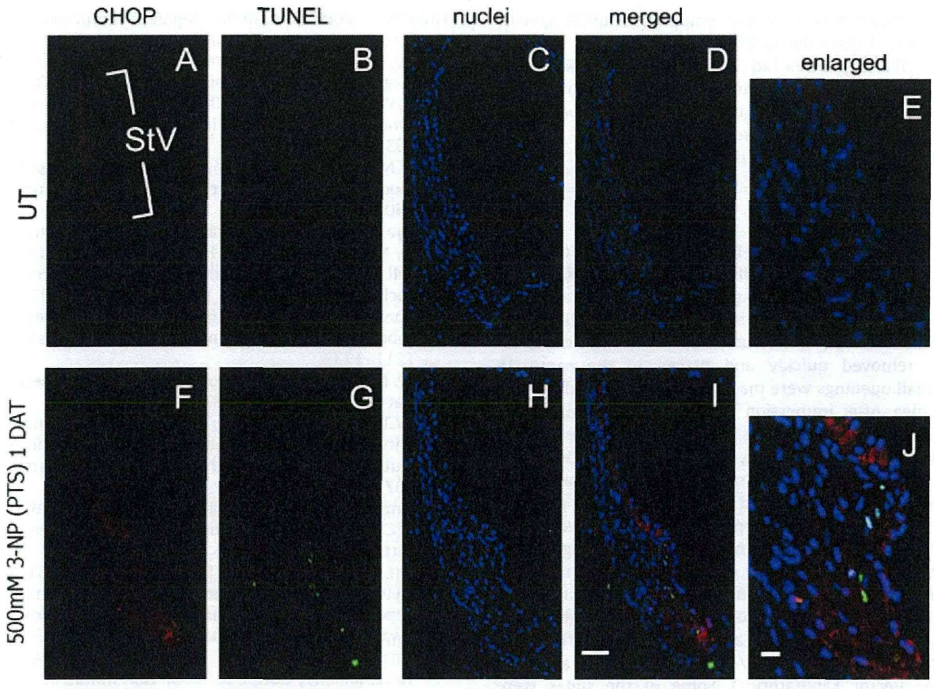

Fig. 5. Concurrent detection of CHOP and apoptosis in the LW after 3-NP treatment. The LW of untreated control rats (UT; A–E) and PTS rats treated with 500 mM 3-NP (F–J) were double-immunostained with antibodies to CHOP (red) and TUNEL (green), and counterstained with DAPI for nuclear staining (blue). Although apoptotic cells were not observed in untreated rats (B, D, and E), apoptosis was detected in the area of type II and type IV fibrocytes in PTS rats 1 day after 3-NP treatment (PTS rats 1 DAT; G) where the CHOP signal was enhanced (F, I, J). E and J were enlarged images of spiral prominence of D and H, respectively. StV; stria vascularis. Scale bar = 50 μm (A–D, F–I) and 10 μm (E, J). (For interpretation of the references to color in this figure legend, the reader is referred to the web version of the article.)

Table 1
PCR primers and their target genes used in the study.

Gene	Acc. number	Sequence (5′ > 3′)		Product length (bp)	Annealing temperature (°C)
		Forward	Reverse		
chop	U30186	AGTCTCTGCCTTTCGCCTTT	GCCACTTTCCTCTCATTCTC	382	55.4
atf-4	NM_024403	GCTGCCCCCTTTACATTCTT	AGCACAAAGCACCTGACTAC	615	54.5
grp78	XM_213908	AACGACCCCTGACAAAAGAC	TAGCCAATTCCTCCTCTCCC	768	57.9
grp94	XM_343192	ACACGGCTTGCTAAACTTCT	CTCTGGCTCTTCCTCTACCT	771	54.2
gapdh	M17701	GCCAAAAGGGTCATCATCTC	GCCTCTCTCTTGCTCTCAGT	715	55.5

Abbreviations: Acc. number: accession number; *chop*: C/EBP homologous protein; *atf-4*: activating transcription factor-4; *grp78* and *grp94*: glucose-regulated protein 78 and 94; *gapdh*: glyceraldehyde-3-phosphate dehydrogenase.

cycle of 12 h and humidity of 55% at 23 °C, with free access to food and water for at least 7 days before use. In these rats, hearing loss was induced by surgical administration of different concentrations of 3-NP onto the inner ear (Hoya et al., 2004). Before surgery, the rats were anesthetized with pentobarbital (40–50 mg/kg, i.p.) or pentobarbital (20–25 mg/kg, i.p.), ketamine (40–60 mg/kg, i.p.) and xylazine (4–6 mg/kg, i.p.). An incision was made posterior to the left pinna near the external meatus after local administration of lidocaine (1%). The left otic bulla was opened to approach the round window niche. The tip of a polyethylene tube (PE10, Becton Dickinson & Co., Franklin Lakes, NJ) was drawn to a fine tip in a flame and gently inserted into the round window niche. 3-NP (Sigma, St. Louis, MO) was dissolved in saline at 300 mM or 500 mM and the pH was adjusted to 7.4 with NaOH. Each 3-NP solution (3 μL) was administered with a syringe pump. Following 3-NP treatment, a tiny piece of gelatin was placed on the niche to keep the solution in the niche during head movement after awakening from anesthesia, and the wound was closed (Hoya et al., 2004; Okamoto et al., 2005). All the experimental procedures were performed in accordance with guidelines from the National Tokyo Medical Center, and were approved by the Animal Care and Use Committee of the Institute. Adequate measures were taken to minimize pain or discomfort of experimental animals.

4.2. Measurement of auditory brainstem response

ABRs were recorded from each rat before 3-NP treatment, and 3 h, 6 h, 1, 2, 3 and 7 days after 3-NP treatment. Pure tone bursts of 8 kHz and 20 kHz (0.2 ms rise/fall time 1 ms flat segment) were used, and auditory thresholds in the treated ear were measured at the same time point using incremental steps of 5 dB. Details of ABR recording were previously described (Hoya et al., 2004).

4.3. Semi-quantitative reverse transcription PCR

After the rats were anesthetized from each rat before 3-NP treatment, and 3 h, 6 h, 1, 2, 3 and 7 days after 3-NP treatment ($n = 5$), temporal bones were quickly removed and immersed in RNA later (Takara Bio, Shiga, Japan) on ice, followed by dissection of the middle turn of the LW. Total RNA was isolated using TRIzol reagent (cultural gen, Carlsbad, CA) according to the manufacturer's protocol. Total RNA was extracted by DEPC-treated water and the purity of total RNA was measured with a UV/visible spectrophotometer (Ultrospec 2100 pro; Amersham Pharmacia Biotech, Piscataway, NJ) by the ratio of OD_{260}/OD_{280}. First-strand cDNA synthesis was performed using 100 ng of total RNA and oligo$(dT)_{12-18}$ primers in a total volume of 20 μL according to the SuperScript III RNase H^- Reverse Transcriptase protocol (cultural gen). We used PCR primers specific for *chop*, *atf-4*, glucose-regulated protein *grp78* and *grp94*, and *gapdh*. The sequences of the PCR primers, sizes of the predicted PCR products, and the annealing temperature are listed in Table 1. The target genes were amplified in 25 μL of reaction containing 2.5 μL of diluted cDNA, 0.2 μM of each dNTP, 0.4 μM of each primer, 0.625 U of Taq DNA polymerase (Sigma) and 1× buffer (10 mM Tris–HCl (pH 8.3), 50 mM KCl, 1.5 mM $MgCl_2$ and 0.001% gelatin). PCR was conducted at 94 °C for 5 min, 30 cycles of 94 °C for 1 min, the specific annealing temperature for 1 min, and 72 °C for 2 min, followed by 72 °C for 10 min, and then 10 μL of each PCR product was analyzed by 1% agarose gel electrophoresis in Tris–acetate-EDTA buffer. PCR products were electrophoresed and visualized using ethidium bromide. The images were captured by CS Analyzer (Atto, Tokyo, Japan).

4.4. Quantitative real-time RT-PCR analysis

qPCR was performed according to manufacturer's protocols for the ABI PRISM 7000 Sequence Detection System (Applied Biosystems, Foster City, CA). The